Improved Accuracy of Velocity Estimation for Cruising Ships by Temporal Differences Between Two Extreme Sublook Images of ALOS-2 Spotlight SAR Images With Long Integration Times

Takero Yoshida, *Member, IEEE*, and Kazuo Ouchi, *Senior Member, IEEE*

***Abstract*—A method for improving the estimation accuracy of the velocity of cruising ships is proposed using synthetic aperture radar (SAR) sublook images in the spotlight mode. The main purpose of spotlight SAR is to obtain high resolution utilizing longer integration times than those of other imaging modes, and the proposed method is based on these long integration times. The principal methodology is to produce successive N sublook images of a cruising ship, where N is more than approximately 10. The positions of the look-1 and look-N subimages differ by a substantial distance proportional to the cruising speed and the long interlook time difference. The distance, and hence the velocity of the cruising ship, can be computed from the cross-correlation function of these two sublook images with improved accuracy compared with other modes. We tested using PALSAR-2 spotlight subimages with $N = 2$, 10, and 20, and the results are compared with the automatic identification system data. Five images of ships cruising close to the azimuth direction were tested; the best result was obtained for the 10-look images with an average error of 13.8%, followed by 17.9% and 40.5% errors for the 20- and 2-look images, respectively. The reason is also given for the best result of the 10-look case over the 20-look case.**

***Index Terms*—Spotlight mode, sublook processing, synthetic aperture radar (SAR), velocity of cruising ships.**

I. Introduction

BECAUSE of all-weather and day-and-night imaging capability, synthetic aperture radar (SAR) has been used effectively for monitoring the vast ocean where *in-situ* data collection is difficult [1]. Apart from the natural oceanic phenomena, ship detection is one of the major issues in the maritime domain awareness, and many studies have been reported such as ship detection [2]–[9] and classification of ships [10]–[13]. In addition, multilook processing was applied to improve ship detection [14], [15]. Meanwhile, estimating the velocity of cruising ships is also important for providing further information. To date, several methods have been proposed for velocity measurement, including those by along-track interferometric SAR (ATI SAR) [16]–[23]. Although ATI SAR can measure only the range velocity component, multichannel SAR [24] and dual-beam ATI SAR with two squint beams [25], [26] to obtain multiple velocity components. In addition to this, Ouchi *et al.* [27] proposed a theory of multiaperture ATI SAR (MA-ATI SAR) to estimate velocity utilizing multi-/sublook processing applied to the conventional ATI SAR data [28], [29].

Apart from the above methods, it was reported that Doppler parameters can be utilized for surveying velocity of ships [30]. On the other hand, another simple robust method is based on the azimuth image shift where the image of a ship with a range velocity component is displaced in the azimuth direction from the image of its ship wake [31]–[33]. The problem, however, is that ship wakes are not always visible, and the application is limited. Another method was suggested to use the images acquired by TerraSAR-X and TanDEM-X in tandem with a large along-track baseline configuration [34]. Although it is simple, well-controlled two SAR platforms are required.

In this paper, we propose a simple method to estimate the velocity of cruising ships using a single SAR in the spotlight mode. The novelty of this article is the utilization of spotlight data. The main purpose of spotlight SAR is to achieve high spatial resolution in the azimuth direction using a long integration time compared with that of other modes such as the Stripmap mode. For example, the azimuth resolution of L-band PALSAR-2 onboard ALOS-2 is 1 m in the spotlight mode with the integration time of 20–30 s; while in the stripmap mode, the resolution is 3–10 m with the integration time of around 10 s [35]. In this research, aforementioned long azimuth integration time is an important factor. For the same resolution, the required synthetic aperture time for the stripmap mode can be the same as the spotlight mode. After this, the spotlight and stripmap modes are discussed, however, it is the case that focuses on ALOS-2/PALSAR-2.

Now, if a ship moves during this long integration time, the spotlight image is blurred and degraded. On the other hand, the

Manuscript received May 23, 2021; revised July 5, 2021, September 1, 2021, and October 26, 2021; accepted November 9, 2021. Date of publication November 11, 2021; date of current version November 24, 2021. This work was supported by the Grants-in-Aid Scientific Research of the Japan Society for the Promotion of Science (JSPS KAKENHI) under Grant JP20K14961 and in part by the director encourage project at the Institute of Industrial Science, The University of Tokyo. *(Corresponding author: Takero Yoshida.)*

Takero Yoshida is with the Department of Ocean Sciences, Tokyo University of Marine Science and Technology, Tokyo 108-8477, Japan, and also with the Institute of Industrial Sciences, The University of Tokyo, Kashiwa-shi 277-8574, Japan (e-mail: tyoshida@iis.u-tokyo.ac.jp).

Kazuo Ouchi is with the Institute of Industrial Sciences, The University of Tokyo, Kashiwa-shi 277-8574, Japan (e-mail: ouchi_sar@yahoo.co.jp).

Digital Object Identifier 10.1109/JSTARS.2021.3127214

distance over which the ship propagates is long in comparison with that in the stripmap mode of short integration times. By taking this as an advantage, the proposed method is to estimate the velocity of cruising ships with increased accuracy by applying multilook processing to the spotlight data. The principal theory is, thus, based on the positions of a moving ship, which differ by the substantial distance between the start and end of the integration time in the spotlight mode. The measurement process is, first, *N*-look processing is applied to the spotlight data, producing successive *N*-look subimages where *N* is more than about 10 depending on the integration time. Then, from the positions of look-1 and look-*N* subimages, the cruising speed, direction, and hence the velocity of the ship can be estimated.

In order to validate the theory, we processed 2-, 10-, and 20-look subimages acquired by the PALSAR-2 over the southern waters of Tokyo Bay, Japan. The results are compared with the automatic identification system (AIS). It should be noted, at this stage, that due to a short integration time of individual sublook, the spatial resolution of sublook images is decreased, but are less blurred and less degraded in comparison with the full-look image. It should also be noted that the sublook images are not fully correlated since the azimuth sublook directions are opposite between the look-1 and look-*N*, and the difference is large.

In the following, the methodology is described for producing sublook images from a single-look complex (SLC) image. The velocity estimation is then made with two sets of PALSAR-2 data using the cross-correlation function (CCF) of sublook images, followed by discussion and conclusions.

II. Methodology

The sublook processing approach from an SLC image is not a new method, since it had been used previously for target detection [36]–[38]. The sublook image is defined as an image formed by a portion of the full bandwidth. As a consequence, the resolution of the sublook image is lower than the original full-look image proportional to 1/*N*. It is a useful method since the sublook processing requires only SLC images without SAR raw data and SAR processor.

For example, Brekke *et al*. [36] extracted sublook images from SLC images with partially overlapped subapertures to improve the subaperture cross-correlation magnitude for ship detection. The theory is based on the assumption that the sea surface has very short decorrelation times compared with the center time difference between subapertures. However, Ouchi and Wang [39] showed theoretically and experimentally using JERS-1 and RADARSAT SAR data that the interlook cross-correlation depends only on the subaperture weighting function and is independent of the temporal correlation of sea surface.

Sanjuan-Ferrer *et al*. [37] also examined both the partially over-lapped and nonoverlapped subimages for a point-like bright target on land. They considered the techniques of sublook coherence, entropy, phase variance, and generalized likelihood ratio test (GLRT). TerraSAR-X data over the glacier in Greenland were used to compare the four techniques, yielding that the GLRT outperformed the others. However, the data they used were in the X-band Stripmap mode, and the azimuth bandwidth was narrower than those of spotlight mode and L-/C-band data. This is, indeed, the main theme of the present work for improving the detection accuracy with L-band PALSAR-2 data at the spotlight mode of long integration times.

Marino *et al*. [38] compared the ship detection algorithms including sublook coherence, cross-correlation, entropy, and GLRT in both azimuth and range directions with extensive ground-truth data of AIS in the North Sea and Tokyo Bay. They concluded that the best algorithm is GLRT with large signal-to-noise ratio (SNR) among the others. But, again, the data used were in the polarimetric mode of the TerraSAR-X (Dual), RADARSAT-2 (Quad), and ALOS-PALSAR (Quad). Although the polarimetric mode of shorter azimuth integration times than the spotlight mode, the results of Marino *et al.* [38] showed that the HV-polarization is better than the other polarizations. This is an expected result since the radar backscatter from the sea surface is small at cross-polarization than copolarization [40].

It is also well known that the radar backscatter from the sea surface increases with decreasing incidence angles at co-polarization while the increase at cross-polarization is relatively uniform [40]. Vachon and Wolfe [41] reported the results of ship detection by C-band ENVISAT-ASAR data with 300–670 ships of different sizes and AIS data. Their results indicate that at the incidence angle $\theta_{\mathrm{T}} \sim 33°$, the SNR increased by 4 dB from small ships (length $<$100 m) to large ships (length $>$160 m) for both the co- and cross-polarizations, and that, on average, the SNR of the cross-polarization is larger at θ_{T} than co-polarization, but the SNR of the co-polarization becomes larger with increasing incidence angles from θ_{T}.

Although the above observations are based on the StripMap and PolSAR data, in this article, the most important and novel part is the utilization of sublook processing on spotlight SAR data. The increased accuracy can be expected by the proposed method using the spotlight SAR data of longer integration times. Here, we show the process to estimate velocity by means of sublook processing on spotlight SAR data.

Fig. 1 shows the flowchart of the proposed method to estimate the velocity of a cruising ship utilizing sublook processing of a spotlight SAR image. First, an SLC image is Fourier transformed, yielding a full-look image spectrum. This spectrum is divided into *N* sub-spectra. To extract a look-1 subimage, for example, the full spectrum is zero-padded except the look-1 subspectrum, and the inverse Fourier transform of this subspectrum yields the look-1 sub-image as illustrated in Fig. 2. Fig. 2 also shows the look-*N* sub-image produced by the IFT of the look-*N* sub-spectrum.

Now, back to the flowchart of Fig. 1, after extracting the second sublook image by repeating the processes labeled 4 to 6, we have two sublook images of different center times. As depicted in Fig. 2, these sublook images of the cruising ship are separated by the azimuth displacement, L_{a}, and it is given by

$$L_a = V_a \Delta t \tag{1}$$

where V_a is the azimuth velocity component of the cruising speed and Δt is the interlook time difference. Since the interlook time difference and cruising direction are known, the cruising

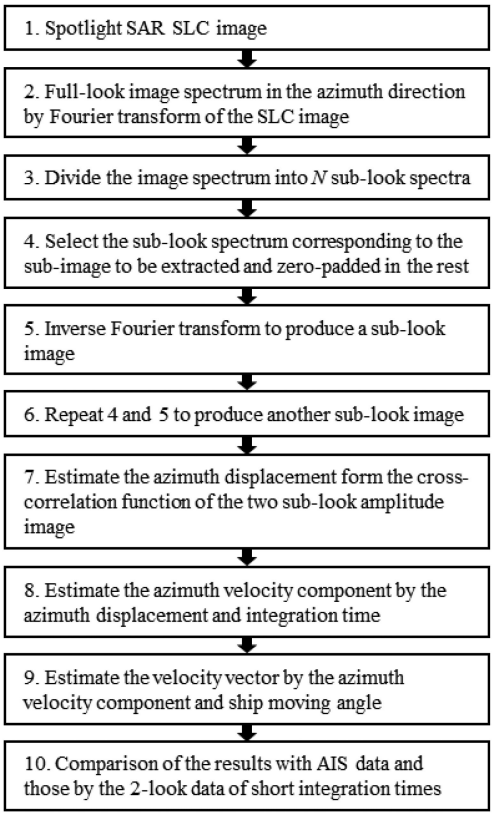

Fig. 1. Flowchart of estimating the velocity of a cruising ship by sublook processing applied to the spotlight SAR SLC image.

velocity can be estimated from the CCF of the two sublook amplitude or intensity images. Then, the results of the interlook CCF and autocorrelation function (ACF) of one sublook are examined. Note that the correlation function represents the degree of similarity between two different data. For instance, in Fig. 2, ACF shows the correlation between sublook 1 and sublook 1, and therefore, the peak is shown at the center of the image, while CCF is between sublook 1 and sublook *N*, thus the peak is shifted from the ACF image due to ship velocity. The comparison with ACF and CCF is understandable to obtain the difference, however, the ACF step can be skipped if this point is kept in mind during the analytical process.

The shift of the CCF peak position from the center of the coordinate axes provides the displacement of the ship during the interlook time difference, and the velocity vector can be estimated. The azimuth velocity component can be estimated from (1). As to the range component, we had, in this preliminary study, only two sets of PALSAR-2 spotlight images where almost all ships were cruising in the azimuth direction. Although two ships appear to be propagating in the off-azimuth direction with small angles, the interlook position differences in the range direction can not be detected by the present method. Nevertheless, we can estimate the velocity vector, $\boldsymbol{V}$, from the azimuth velocity component and the shape of a ship as shown in Fig. 3, and

$$V = \frac{V_a}{\cos\,\theta} \tag{2}$$

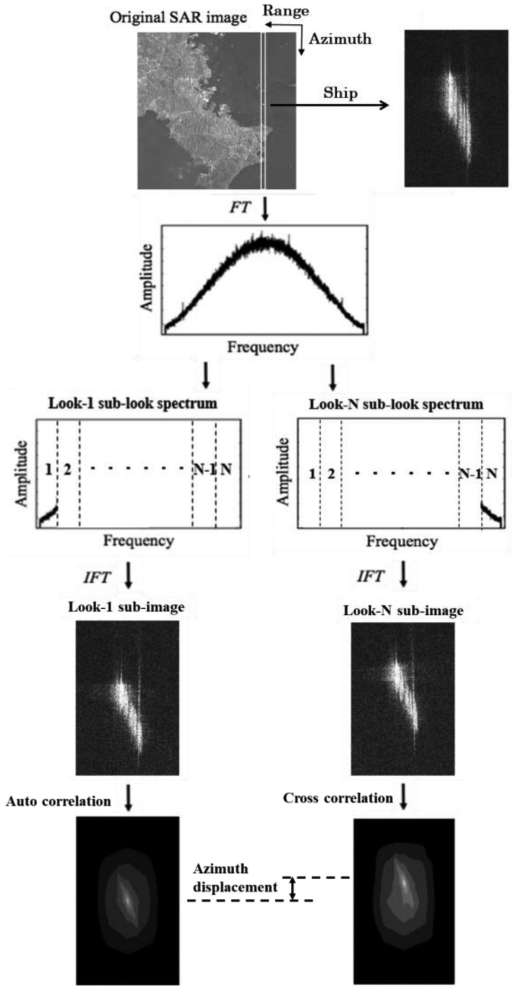

Fig. 2. Illustrating the *N*-look sublook processing in the azimuth direction from spotlight SAR SLC data, showing the look-1 and look-*N* sublook images as an example. The azimuth displacement can be obtained by the cross-correlations of different sublook images.

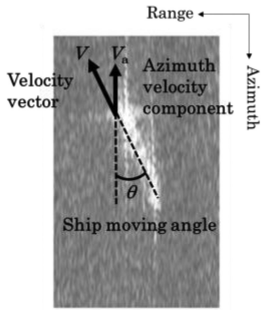

Fig. 3. Estimate the velocity vector by the azimuth velocity component and ship moving angle.

where θ is the ship moving angle from the azimuth direction.

As noted previously, the spatial resolution of subimages is lower than that of the full-look image, but image degradation by the ship's motion is less severe. In addition, the degradation, that is, blurring and shapes of subimages are, to some extent, different due also to the different azimuth sublook angles, resulting in a decrease of the degree of correlation (coherence). However, the

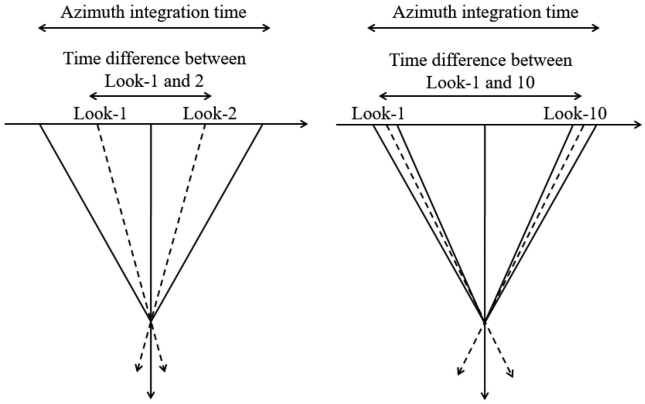

Fig. 4. Calculate the time difference between sub looks. For instance, two cases of look-1 and -2, and look-1 and -10 are depicted.

TABLE I
SAR DATA SPECIFICATION (SCENE 1)

Scene ID	ALOS2047162919-150408
Mode	Spotlight
Observation date and time	2015-04-08 02:22
Polarization	HH
Azimuth duration time	23 s

TABLE II
SAR IMAGE SPECIFICATION (SCENE 2)

Scene ID	ALOS2052782911-150516
Mode	Spotlight
Observation date and time	2015-05-16 02:36
Polarization	VV
Azimuth duration time	29 s

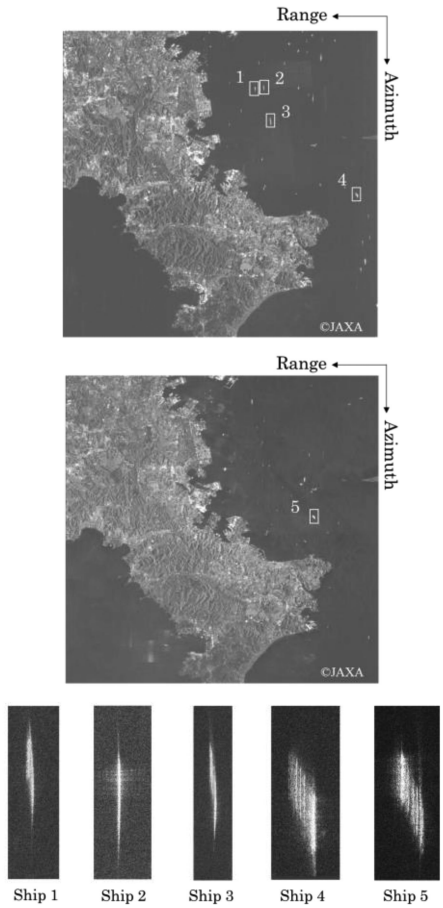

Fig. 5. PALSAR-2 spotlight images (upper) and five full-look images of ships for analyses (bottom). The ship images are enlarged arbitrarily at the bottom columns.

decrease does not appear significant at first glance. In fact, the sublook images are correlated sufficiently for the purpose, as detailed in the following section.

Using velocity estimation, the results are compared with AIS data. The primary contribution of the proposed theory is the improved estimation accuracy using spotlight SAR with long integration times as compared with other modes of shorter integration times such as stripmap mode. However, there have been no simultaneous data of different modes. The same spotlight data are then used by applying two-look processing with the integration time close to the stripmap mode. In order to calculate the time difference between sublooks, Fig. 4 is depicted briefly. As shown in the example of 10 looks in Fig. 4, the time difference is close to the original long azimuth integration time, however, it is short in the case of two looks. The time difference of two looks in the spotlight mode is similar to that of 10 or 20 looks in the stripmap mode for the case of ALOS-2/PALSAR-2.

III. RESULTS AND DISCUSSION

A. SAR Data

In order to validate the proposed method, two sets of ALOS-2 L-band PALSAR-2 data in the spotlight mode are used as listed in Tables I and II. They are labeled as scene 1 and scene 2, respectively. Both the data are in the descending mode with the integration times of 23 and 29 s, respectively (We cited from AUIG2 ALOS-2/ALOS User Interface Gateway).[1] The resolution is 1 m $\times$ 3 m in the azimuth and range directions, respectively, and the pixel sizes are the same in both directions.

The area of interest is the western coast of the Miura peninsula in Tokyo Bay, Japan as shown in Fig. 5. Tokyo Bay is one of the busiest ports, and many ships can be seen in the figure; there also are some faint ghost images due to azimuth ambiguity and/or radio frequency interference.

In the present study, five cruising ships, of which the full-look images are shown in Fig. 5, were used for analyses. The images are degraded due to the movement of ships. The image pixels are 300×900, 300×900, 300×1600, 300×1400, 400×600 for ships 1 to 5, respectively. In particular, the images are smeared in the azimuth direction because of the long integration times of spotlight mode as mentioned earlier. These images were divided into 2, 10, and 20 sublook images in the azimuth direction by the sublook processing as in Fig. 2.

Examples of the sublook images in terms of ships 1 and 5 are shown in Figs. 6 and 7 for the cases of 2- and 20-look processing,

[1][Online]. Available: https://auig2.jaxa.jp/ips/home

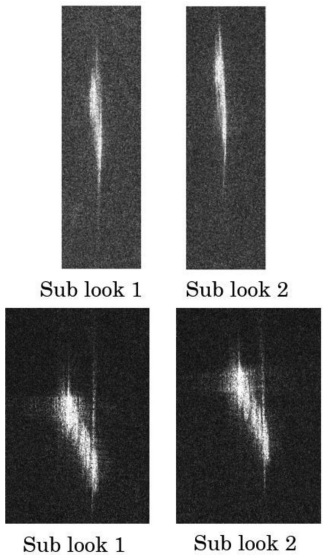

Fig. 6. Examples of sublook images of cruising ships for the ships 1 (upper) and 5 (bottom) in the case of two-look processing. The image pixel sizes are 300 × 900 and 400 × 600 for ships 1 and 5.

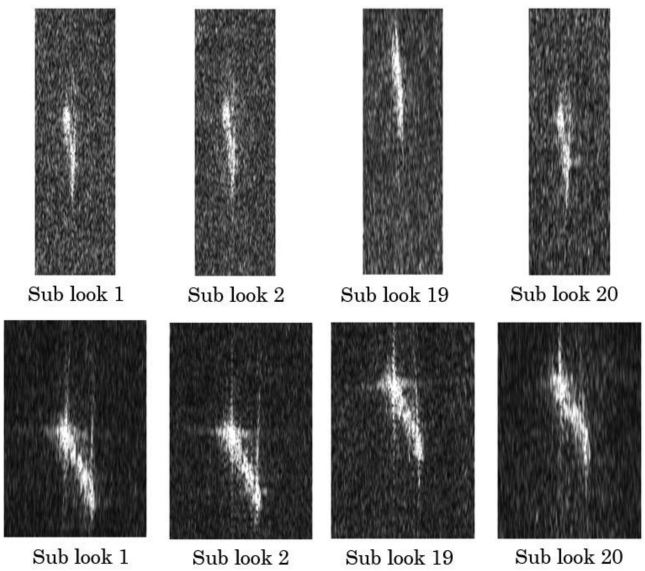

Fig. 7. Examples of sublook images of the ships 1 (upper) and 5 (bottom) in the case of 20 sublook processing.

respectively. As in both the figures, the subimages show the difference in the azimuth position due to ship movement during the interlook azimuth time. It is obvious that the azimuth shift of 20-look is larger than that of 2-look though the image resolution is worse. As expected, the differences of the interlook image positions are clearly larger for the 20-look case than 2-look case.

In the case of 20 subimages of ship 1 in the upper row of Fig. 7, the azimuth position of the sublook 20 image is similar to that of the sublook 1 image. In the spotlight mode, the SAR is squinted to look forward and backward, then the received signals are superimposed to obtain fine resolution. If the position of a ship is deviated from the center of the SAR image, the center

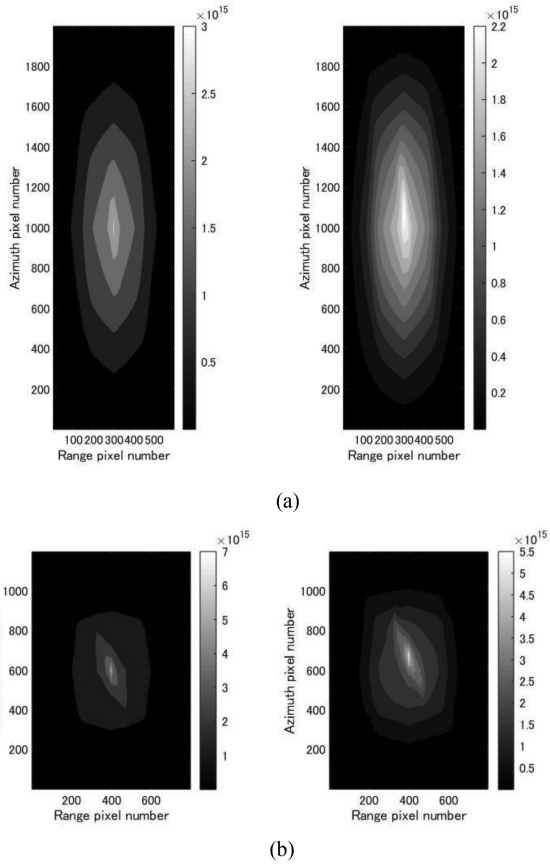

Fig. 8. ACF of sublook image 1 (left), and CCF of sublook images of 1 and 2 (right), for (a) ship 1 and (b) ship 5 with two sublook images. The pixel sizes are double as the original due to two-dimensional correlation, the pixels are 600 × 1800 and 800 × 1200 for ships 1 and 5.

frequency of the azimuth direction may be shifted by the above reason (the upper figures of Fig. 7). However, if the position of a ship is close to the center of the SAR image, it cannot be seen such shift in sublook 20 (the bottom figures of Fig. 7), and therefore the 2 and 19 submages are used for analysis. Similarly, the two and nine subimages are analyzed in the 10 sublook cases.

B. Estimation of Cruising Velocity

We focus on the measurement of the azimuth velocity, since the cruising direction is known from the shape of the ship's image, and hence the velocity vector can be estimated. Another reason is that the cruising direction is predominantly in the azimuth direction in the Tokyo bay where the data were taken.

To calculate accurate azimuth image displacement, the CCF was used for interlook subimages. Examples are shown in Figs. 8 –10 for the cases of 2-look, 10-look, and 20-look processing of the shipping numbers 1 and 5, respectively. The ACF of the sublook 1 image is shown on the left of Fig. 8, and the CCF of the sublook 1 and 2 images on the right. Similarly, the ACF of the sublook 2 image and its CCF with the sublook 9 and 19 images are shown on the left and right of Figs. 9 and 10, respectively. The interlook image displacement can then be calculated from the difference of the peak positions of the ACF and CCF.

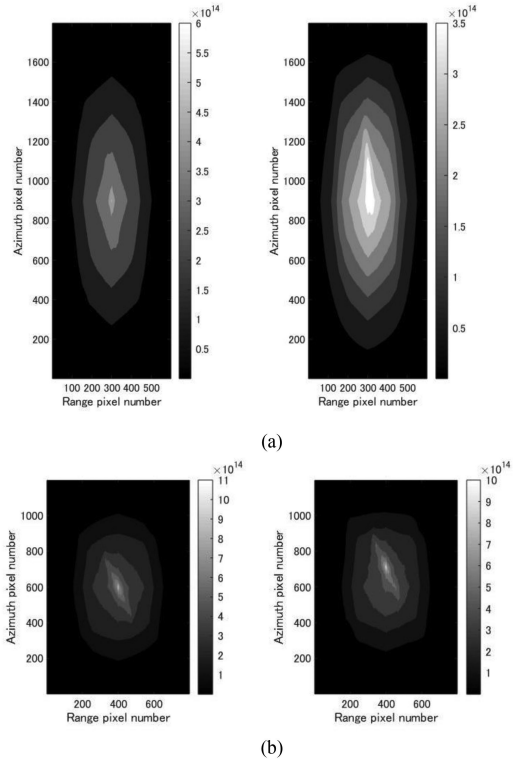

Fig. 9. ACF of sublook image 2 (left), and CCF of sublook images of 2 and 9 (right), for (a) ship 1 and (b) ship 5 with 10 sublook images. The pixel sizes are as in Fig. 8.

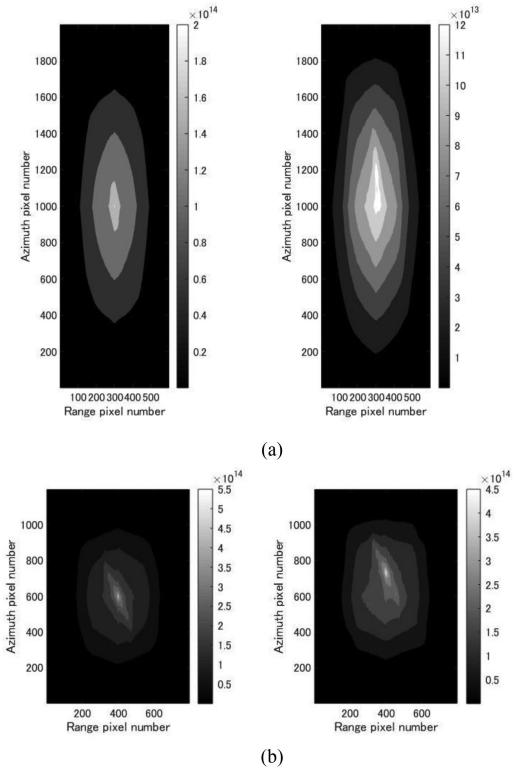

Fig. 10. ACF of sublook image 2 (left), and CCF of sublook images of 2 and 19 (right), for (a) ship 1 and (b) ship 5 with 20 sublook images. The pixel sizes are as in Fig. 8.

TABLE III
TIME DIFFERENCE BETWEEN SUBLOOK IMAGES 1 AND N (2, 10, 20)

Scene No.	2-look (s)	10-look (s)	20-look (s)
1	11.5	16.1	19.6
2	14.5	20.3	24.7

TABLE IV
ESTIMATED RESULT USING TWO SUBLOOK IMAGES AND AIS DATA

No.	Velocity by AIS (m/s)	Velocity (m/s)	Error (%)
1	5.1	2.4	52.9
2	7.6	4.5	40.8
3	6.4	4.2	34.4
4	6.5	4.1	36.9
5	6.7	4.2	37.3
			Ave. 40.5

TABLE V
ESTIMATED RESULT USING 10 SUBLOOK IMAGES AND AIS DATA

No.	Velocity by AIS (m/s)	Velocity (m/s)	Error (%)
1	5.1	4.8	5.9
2	7.6	7.3	3.9
3	6.4	6.8	6.3
4	6.5	5.0	23.1
5	6.7	4.7	30.0
			Ave. 13.8 %

TABLE VI
ESTIMATED RESULT USING 20 SUBLOOK IMAGES AND AIS DATA

No.	Velocity by AIS (m/s)	Velocity (m/s)	Error (%)
1	5.1	4.8	5.9
2	7.6	6.0	21.1
3	6.4	7.0	9.4
4	6.5	4.6	29.2
5	6.7	5.1	23.9
			Ave. 17.9 %

As listed in Table III, the time differences between sublook images were roughly 11.5–14.5 s, 16.1–20.3 s, and 19.6–24.7 s for the 2-look, 10-look, and 20-look cases, respectively. The pixel spacing was 0.625 m. Thus, from these interlook time and correlation peak differences, the azimuth velocity components can be computed.

Next, the ship cruising direction is examined from the shapes of the ships' images. While the ships 1 and 2 were cruising almost in the azimuth direction, the ships 3, 4, and 5 were cruising at angles from the azimuth direction as can be seen in Fig. 4. These angles are 10°, 25°, and 25° for ships 3, 4, and 5, respectively. By taking into consideration the cruising directions, the cruising velocities of all five ships can finally be estimated as shown in Tables IV–VI, where the velocities from the AIS data as the ground-truth are also listed for comparison.

The comparison of the results with AIS data shows that the range of errors is 34.4–52.9% for the two-look case, and 3.9–30.0% and 5.9–29.2% for the 10-look and 20-look cases, respectively. The average errors are 40.5%, 13.8%, and 17.9% for the 2-look, 10-look, and 20-look cases, respectively. Thus, substantial improvement in velocity estimation is made using the spotlight data with increased sublook numbers in comparison with the simulated stripmap mode of short interlook times.

The most accurate estimation is the 10-look case, followed by the 20-look and 2-look cases. We expected that the 20-look case is the most accurate although the difference from the 10-look case is not large. This may be because the azimuth sublook angles of the 20-look case are larger than those of the 10-look case, resulting in a larger difference between the 2-look and 19-look subimages. In the case of the 10-look case, the estimation errors of ships 4 and 5 are relatively large. It is considered that the estimation can be accurately applied for ships cruising close to the azimuth direction. The other reason may be because of the change of cruising direction during the interlook time. The present method is based on the assumption that ships do not change their course during the observation. If the cruising direction changes during the interlook azimuth time, the difference in image structure is large, and the interlook images are less correlated. Longer the interlook azimuth time is, the larger the interlook image difference becomes. In fact, the cruising directions of the ship 2 sublook images in the 20-look case appear slightly different. Further, the cruising direction of ship 4 is about 25°, so that the azimuth velocity component is small, causing an increased potential error.

In the present preliminary study, only five ships cruising mainly in the azimuth direction in spotlight SAR data were used. As a future study, increased numbers of ships cruising at various speeds and directions, as well as the other observation mode are required. Especially, the method can be adopted for ships cruising close to the azimuth direction, therefore, the quantitative evaluation in terms of the ship that has both radial and azimuth velocity components. In particular, if the ship moving angle is close to the range direction, the current estimation could be influenced. In addition, signal-to-noise ratio (SNR) can be another factor to affect the analysis. The moving ship images are sometimes blurred in the subimages, and if SNR is low, it can be a barrier to extract the ship motion from the subimages. Also, the other ground truth data such as ocean current and direction of movement may provide us additional insight on this method. They are required to discuss as a next step.

IV. Conclusion

In this article, preliminary results are presented on the improvement of velocity estimation of cruising ships by applying sublook processing to the SAR data in the spotlight mode. The principle is to utilize the long azimuth integration times of the spotlight data as compared with, for example, the stripmap data. The interlook time difference between the well-separated subimages in the number of sublooks is, therefore, long, and the subimage positions of a cruising ship are also well-separated. To test the theory, 2, 10, and 20 sublook images of five ships are produced in the two sets of PALSAR-2 spotlight data over the Tokyo bay, Japan. Comparison with the AIS data shows substantial improvement in velocity estimation by 10-look processing with a 13.8% average error in comparison with the two-look case of 40.5% error. Further study is in progress using an increased number of ships cruising with different speeds and directions to clarify the estimation accuracy for various kinds of moving ships.

Acknowledgment

PALSAR-2 data are the property of the Japan Aerospace Exploration Agency (JAXA). The Spotlight SAR images used in this study are scene ID: ALOS2047162919-150408 and ALOS2052782911-150516. AIS data were provided by Toyo-shingo-tsushinsha (TST) Corporation.

References

[1] K. Ouchi, "Recent trend and advance of synthetic aperture radar with selected topics," *Remote Sens.*, vol. 5, no. 2, pp. 716–807, 2013.

[2] S. Brusch, S. Lehner, T. Fritz, M. Soccorsi, A. Soloviev, and B. van Schie, "Ship surveillance with TerraSAR-X," *IEEE Trans. Geosci. Remote Sens.*, vol. 49, no. 3, pp. 1092–1103, Mar. 2011.

[3] E. Makhoul, S. V. Baumgartner, M. Jäger, and A. Broquetas, "Multichannel SAR-GMTI in maritime scenarios with F-SAR and TerraSAR-X sensors," *IEEE J. Sel. Topics. Appl. Earth Observ. Remote Sens.*, vol. 8, no. 11, pp. 5052–5067, Nov. 2015, doi: 10.1109/JSTARS.2015.2438898.

[4] C. Wang, S. Jiang, H. Zhang, F. Wu, and B. Zhang, "Ship detection for high-resolution SAR images based on feature analysis," *IEEE Geosci. Remote Sens. Lett.*, vol. 11, no. 1, pp. 119–123, Jan. 2014, doi: 10.1109/LGRS.2013.2248118.

[5] A. Marino, M. J. Sanjuan-Ferrer, I. Hajnsek, and K. Ouchi, "Ship detection with spectral analysis of synthetic aperture radar: A comparison of new and well-known algorithms," *Remote Sens.*, vol. 7, no. 5, pp. 5416–5439, 2015.

[6] A. Marino and I. Hajnsek, "Ship detection with TanDEM-X data extending the polarimetric notch filter," *IEEE Geosci. Remote Sens. Lett.*, vol. 12, no. 10, pp. 2160–2164, Oct. 2015, doi: 10.1109/LGRS.2015.2453235.

[7] W. Ao, F. Xu, Y. Li, and H. Wang, "Detection and discrimination of ship targets in complex background from spaceborne ALOS-2 SAR images," *IEEE J. Sel. Top. Appl. Earth Observ. Remote Sens.*, vol. 11, no. 2, pp. 536–550, Feb. 2018.

[8] X. Zhang *et al.*, "A lightweight feature optimizing network for ship detection in SAR image," *IEEE Access*, vol. 7, pp. 141662–141678, 2019, doi: 10.1109/ACCESS.2019.2943241.

[9] M. Tello, C. Lopez-Martinez, and J. J. Mallorqui, "A novel algorithm for ship detection in SAR imagery based on the wavelet transform," *IEEE Geosci. Remote Sens. Lett.*, vol. 2, no. 2, pp. 201–205, Apr. 2005, doi: 10.1109/LGRS.2005.845033.

[10] X. Xing, K. Ji, H. Zou, W. Chen, and J. Sun, "Ship classification in TerraSAR-X images with feature space based sparse representation," *IEEE Geosci. Remote Sens. Lett.*, vol. 10, no. 6, pp. 1562–1566, Nov. 2013, doi: 10.1109/LGRS.2013.2262073.

[11] H. Lang, J. Zhang, T. Zhang, D. Zhao, and J. Meng, "Hierarchical ship detection and recognition with high-resolution polarimetric synthetic aperture radar imagery," *J. Appl. Remote Sens.*, vol. 8, no. 1, May 2014, Art. no. 083623, doi: 10.1117/1.JRS.8.083623.

[12] S. Chen, H. Wang, F. Xu, and Y. Jin, "Target classification using the deep convolutional networks for SAR images," *IEEE Trans. Geosci. Remote Sens.*, vol. 54, no. 8, pp. 4806–4817, Aug. 2016, doi: 10.1109/TGRS.2016.2551720.

[13] M. Rodger and R. Guida, "Classification-aided SAR and AIS data fusion for space-based maritime surveillance," *Remote Sens.*, vol. 13, no. 1, Dec. 2020, Art. no. 104.

[14] K. Ouchi, S. Tamaki, H. Yaguchi, and M. Iehara, "Ship detection based on coherence images derived from cross correlation of multilook SAR images," *IEEE Geosci. Remote Sens. Lett.*, vol. 1, no. 3, pp. 184–187, Jul. 2004.

[15] S.-I. Hwang and K. Ouchi, "On a novel approach using MLCC and CFAR for the improvement of ship detection by synthetic aperture radar," *IEEE Geosci. Remote Sens. Lett.*, vol. 7, no. 2, pp. 391–395, Apr. 2010.

[16] R. M. Goldstein and H. A. Zebker, "Interferometric radar measurement of ocean surface currents," *Nature*, vol. 328, no. 6132, pp. 707–709, 1987.

[17] R. M. Goldstein, T. P. Barnett, and H. A. Zebker, "Remote sensing of ocean currents," *Science*, vol. 246, no. 4935, pp. 1282–1285, 1989.

[18] R. Romeiser, "Current measurements by airborne along-track insar: Measuring technique and experimental results," *IEEE J. Ocean. Eng.*, vol. 30, no. 3, pp. 552–569, Jul. 2005.

[19] R. Romeiser *et al.*, "Current measurements by SAR along-track interferometry from a space shuttle," *IEEE Trans. Geosci. Remote Sens.*, vol. 43, no. 10, pp. 2315–2324, Oct. 2005.

[20] R. Romeiser, S. Suchandt, H. Runge, U. Steinbrecher, and S. Grünler, "First analysis of TerraSAR-X along-track insar-derived current fields," *IEEE Trans. Geosci. Remote Sens.*, vol. 48, no. 2, pp. 820–829, Feb. 2010.
[21] R. Romeiser, "The future of SAR-based oceanography: High-resolution current measurements by along-track interferometry," *Oceanography*, vol. 26, no. 2, pp. 92–99, 2013.
[22] P. W. Vachon, J. W. M. Campbell, A. L. Gray, and F. W. Dobson, "Validation of along-track interferometric SAR measurements of ocean surface waves," *IEEE Trans. Geosci. Remote Sens.*, vol. 37, no. 1, pp. 150–162, Jan. 1999.
[23] D. Kim, W. M. Moon, D. Moller, and D. A. Imel, "Measurements of ocean surface waves and currents using L- and C-band along-track interferometric SAR," *IEEE Trans. Geosci. Remote Sens.*, vol. 41, no. 12, pp. 2821–2832, Dec. 2003.
[24] K. Suwa, K. Yamamoto, M. Tsuchida, S. Nakamura, T. Wakayama, and T. Hara, "Image-based target detection and radial velocity estimation methods for multichannel SAR-GMTI," *IEEE Trans. Geosci. Remote Sens.*, vol. 55, no. 3, pp. 1325–1338, Mar. 2017.
[25] S. J. Frasier and A. J. Camps, "Dual-beam interferometry for ocean surface current vector mapping," *IEEE Trans. Geosci. Remote Sens.*, vol. 39, no. 2, pp. 401–414, Feb. 2001.
[26] S. Wollstadt, P. López-Dekker, F. De Zan, and M. Younis, "Design principles and consideration for spaceborne ATI SAR-based observations of ocean surface velocity vectors," *IEEE Trans. Geosci. Remote Sens.*, vol. 55, no. 8, pp. 4500–4519, Aug. 2017.
[27] K. Ouchi, T. Yoshida, and C.-S. Yang, "A theory of multiaperture along-track interferometric synthetic aperture radar," *IEEE Geosci. Remote Sens. Lett.*, vol. 16, no. 10, pp. 1565–1569, Oct. 2019, doi: 10.1109/LGRS.2019.2906104.
[28] T. Yoshida, K. Ouchi, and C. -S. Yang, "Validation of MA-ATI SAR theory using numerical simulation for estimating the direction of moving targets and ocean currents," *IEEE Geosci. Remote Sens. Lett.*, vol. 18, no. 4, pp. 677–681, Apr. 2021, doi: 10.1109/LGRS.2020.2983160.
[29] T. Yoshida, K. Ouchi, and C. -S. Yang, "Application of MA-ATI SAR for estimating the direction of moving water surface currents in pi-sar2 images," *IEEE J. Sel. Topics. Appl. Earth Observ. Remote Sens.*, vol. 14, pp. 2724–2730, 2021, doi: 10.1109/JSTARS.2021.3060008.
[30] A. Renga and A. Moccia, "Use of Doppler parameters for ship velocity computation in SAR images," *IEEE Trans. Geosci. Remote Sens.*, vol. 54, no. 7, pp. 3995–4011, Jul. 2016, doi: 10.1109/TGRS.2016.2533023.
[31] M. D. Graziano, M. D'Errico, and G. Rufino, "Ship heading and velocity analysis by wake detection in SAR images," *Acta Astronaut.*, vol. 128, pp. 72–82, 2016, doi:10.1016/j.actaastro.2016.07.001.
[32] K.-M. Kang and D.-J. Kim, "Ship velocity estimation from ship wakes detected using convolutional neural networks," *IEEE J. Sel. Topics. Appl. Earth Observ. Remote Sens.*, vol. 12, no. 11, pp. 4379–4388, Nov. 2019, doi: 10.1109/JSTARS.2019.2949006.
[33] B. Tings, A. Pleskachevsky, D. Velotto, and S. Jacobsen, "Extension of ship wake detectability model for non-linear influences of parameters using satellite based X-band synthetic aperture radar," *Remote Sens.*, vol. 11, no. 5, Mar. 2019, Art. no. 563.
[34] S. V. Baumgartner and G. Krieger, "Ship detection and motion parameter estimation with TanDEM-X in large along-track baseline configuration," in *Proc. SeaSAR*, 2012.
[35] Japan Aerospace Exploration Agency, "PALSAR-2 level 1.1/2.1/1.5/3.1 CEOS SAR product format description," 2016. [Online]. Available: https://www.eorc.jaxa.jp/ALOS-2/en/doc/fdata/PALSAR-2_xx_Format_CEOS_E_f.pdf
[36] C. Brekke, S. N. Anfinsen, and Y. Larsen, "Subband extraction strategies in ship detection with the subaperture cross-correlation magnitude," *IEEE Geosci. Remote Sens. Lett.*, vol. 10, no. 4, pp. 786–790, Jul. 2013.
[37] M. J. Sanjuan-Ferrer, I. Hajnsek, K. P. Papathanassiou, and A. Moreira, "A new detection algorithm for coherent scatters in SAR data," *IEEE Trans. Geosci. Remote Sens.*, vol. 53, no. 11, pp. 6293–6307, Nov. 2015.
[38] A. Renge, M.-D. Graziano, and A. Moccia, "Segmentation of marine SAR images by sublook analysis and application to sea traffic monitoring," *IEEE Tans. Geosci. Remote Sens.*, vol. 57, no. 3, pp. 1463–1477, Mar. 2019.
[39] K. Ouchi and H. Wang, "Interlook cross-correlation function of speckle in SAR images of sea surface processesd with partially overlapped subapertures," *IEEE Trans. Geosci. Remote Sens.*, vol. 43, no. 4, pp. 695–701, Apr. 2005.
[40] P. W. Vachon and J. Wolfe, "C-band cross-polarization wind speed retrieval," *IEEE Geosci. Remote Sens. Lett.,* vol. 8, no. 3, pp. 456–459, May 2011.
[41] P. W. Vachon and J. Wolfe, "Validation OD ship signatures in envisat ASAR AP mode data using AISLive," Rep. No. TM 2008-005, DRRC, Ottawa, ON, Canada, 2008.

Takero Yoshida (Member, IEEE) received the Ph.D. degree in environmental studies from the Department of Ocean Technology, Policy and Environment, the University of Tokyo, Tokyo, Japan, in 2013.

From 2016 to 2021, he was an Assistant Professor with the Institute of Industrial Science, the University of Tokyo. Since 2021, he is an Associate Professor with Department of Ocean Sciences, Tokyo University of Marine Science and Technology. His research activities include the fields of data and image analysis, ocean monitoring, marine environmental impact assessments, SAR image analysis in water areas, and numerical simulation of electromagnetic scattering from ocean surface.

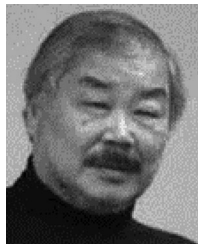

Kazuo Ouchi (Senior Member, IEEE) received the Ph.D. degree from Physics Department, Imperial Collage of Science and Technology, University of London, England, in 1981.

He was a Research Assistant with Imperial Collage, a research associate in King's Collage, and a research fellow with Imperial Collage, University of London from 1980 to 1996. He was a Professor with the Department of Environmental Studies, Hiroshima Institute of Technology, Hiroshima, Japan, from 1996 to 1999. He was a Professor with the Department of Environmental Systems Engineering, Kochi University of Technology, Kochi, Japan, from 1999 to 2006. He was a Professor with the Department of Computer Science, National Defense Academy, Kanagawa, Japan, from 2006 to 2013. After retirement from NDA in March 2013, he was a Research Scientist of the Brain Pool Program with the Korea Institute of Ocean Science and Technology, Busan, Korea. He was a Senior Consulting Manager with IHI Corp., Tokyo, Japan from 2015 to 2020. Currently, he is a senior collaborator with the Institute of Industrial Science, the University of Tokyo, Tokyo, Japan, since 2020. His research interests include SAR/InSAR/PolSAR systems and applications to land and ocean, EM scattering, and microwave/optical remote sensing.